Quantum witness of high-speed low-noise single-photon detection

Lin Zhao,[1] Kun Huang,[1] Yan Liang,[2] Jie Chen,[2] Xueshun Shi,[3] E Wu,[1,4] and Heping Zeng[1]*

[1]*State Key Laboratory of Precision Spectroscopy, East China Normal University, Shanghai 200062, China*
[2]*Shanghai Key Laboratory of Modern Optical System, Engineering Research Center of Optical Instrument and System (Ministry of Education), School of Optical-Electrical and Computer Engineering, University of Shanghai for Science and Technology, Shanghai 200093, China*
[3]*The 41st Institute of China Electronics Technology Group Corporation and Science and Technology on Electronic Test& Measurement Laboratory, Qingdao 266555, China*
[4]*ewu@phy.ecnu.edu.cn*
[*]hpzeng@phy.ecnu.edu.cn

Abstract: We demonstrate high-speed and low-noise near-infrared single-photon detection by using a capacitance balancing circuit to achieve a high spike noise suppression for an InGaAs/InP avalanche photodiode. The single-photon detector could operate at a tunable gate repetition rate from 10 to 60 MHz. A peak detection efficiency of 34% has been achieved with a dark count rate of 9×10^{-3} per gate when the detection window was set to 1 ns. Additionally, quantum detector tomography has also been performed at 60 MHz of repetition rate and for the detection window of 1 ns, enabling to witness the quantum features of the detector with the help of a negative Wigner function. By varying the bias voltage of the detector, we further demonstrated a transition from the full-quantum to semi-classical regime.

References and links

1. N. Namekata, H. Takesue, T. Honjo, Y. Tokura, and S. Inoue, "High-rate quantum key distribution over 100 km using ultra-low-noise, 2-GHz sinusoidally gated InGaAs/InP avalanche photodiodes," Opt. Express **19**(11), 10632–10639 (2011).
2. B. Korzh, W. Lim, R. Houlmann, N. Gisin, M. Li, D. Nolan, B. Sanguinetti, R. Thew, and H. Zbinden, "Provably secure and practical quantum key distribution over 307 km of optical fibre," Nat. Photonics **9**(3), 163–168 (2015).
3. H. Shibata, T. Honjo, and K. Shimizu, "Quantum key distribution over a 72 dB channel loss using ultralow dark count superconducting single-photon detectors," Opt. Lett. **39**(17), 5078–5081 (2014).
4. Y. Liu, T. Y. Chen, L. J. Wang, H. Liang, G. L. Shentu, J. Wang, K. Cui, H. L. Yin, N. L. Liu, L. Li, X. Ma, J. S. Pelc, M. M. Fejer, C. Z. Peng, Q. Zhang, and J. W. Pan, "Experimental measurement-device-independent quantum key distribution," Phys. Rev. Lett. **111**(13), 130502 (2013).
5. M. Ren, G. Wu, E. Wu, and H. Zeng, "Experimental demonstration of counterfactual quantum key distribution," Laser Phys. **21**(4), 755–760 (2011).
6. Y. Liang, J. Huang, M. Ren, B. Feng, X. Chen, E. Wu, G. Wu, and H. Zeng, "1550-nm time-of-flight ranging system employing laser with multiple repetition rates for reducing the range ambiguity," Opt. Express **22**(4), 4662–4670 (2014).
7. M. Ren, X. Gu, Y. Liang, W. Kong, E. Wu, G. Wu, and H. Zeng, "Laser ranging at 1550 nm with 1-GHz sine-wave gated InGaAs/InP APD single-photon detector," Opt. Express **19**(14), 13497–13502 (2011).
8. D. R. Reilly and G. S. Kanter, "High speed lidar via GHz gated photon detector and locked but unequal optical pulse rates," Opt. Express **22**(13), 15718–15723 (2014).
9. S. Chen, D. Liu, W. Zhang, L. You, Y. He, W. Zhang, X. Yang, G. Wu, M. Ren, H. Zeng, Z. Wang, X. Xie, and M. Jiang, "Time-of-flight laser ranging and imaging at 1550 nm using low-jitter superconducting nanowire single-photon detection system," Appl. Opt. **52**(14), 3241–3245 (2013).
10. G. Brida, M. Genovese, and I. Berchera, "Experimental realization of sub-shot-noise quantum imaging," Nat. Photonics **4**(4), 227–230 (2010).
11. L. Xu, E. Wu, X. Gu, Y. Jian, G. Wu, and H. Zeng, "High-speed InGaAs/InP-based single-photon detector with

high efficiency," Appl. Phys. Lett. **94**(16), 161106 (2009).

12. L. Comandar, B. Fröhlich, M. Lucamarini, K. Patel, A. Sharpe, J. Dynes, Z. Yuan, R. Penty, and A. Shields, "Room temperature single-photon detectors for high bit rate quantum key distribution," Appl. Phys. Lett. **104**(2), 021101 (2014).

13. J. Zhang, T. Rob, B. Claudio, and Z. Hugo, "Practical fast gate rate InGaAs/InP single-photon avalanche photodiodes," Appl. Phys. Lett. **95**(9), 091103 (2009).

14. Y. Liang, E. Wu, X. Chen, M. Ren, Y. Jian, G. Wu, and H. Zeng, "Low-timing-jitter single-photon detection using 1-GHz sinusoidally gated InGaAs/InP avalanche photodiode," IEEE Photonics Technol. Lett. **23**(13), 887–889 (2011).

15. Q. Wu, N. Namekata, and S. Inoue, "Sinusoidally gated InGaAs avalanche photodiode with direct hold-off function for efficient and low-noise single-photon detection," Appl. Phys. Express **6**(6), 062202 (2013).

16. E. Bimbard, N. Jain, A. MacRae, and A. Lvovsky, "Quantum-optical state engineering up to the two-photon level," Nat. Photonics **4**(4), 243–247 (2010).

17. B. P. Lanyon, P. Jurcevic, M. Zwerger, C. Hempel, E. A. Martinez, W. Dür, H. J. Briegel, R. Blatt, and C. F. Roos, "Measurement-based quantum computation with trapped ions," Phys. Rev. Lett. **111**(21), 210501 (2013).

18. C. M. Natarajan, L. Zhang, H. Coldenstrodt-Ronge, G. Donati, S. N. Dorenbos, V. Zwiller, I. A. Walmsley, and R. H. Hadfield, "Quantum detector tomography of a time-multiplexed superconducting nanowire single-photon detector at telecom wavelengths," Opt. Express **21**(1), 893–902 (2013).

19. X. Zhou, H. Cable, R. Whittaker, P. Shadbolt, J. O'Brien, and J. Matthews, "Quantum-enhanced tomography of unitary processes," Optica **2**(6), 510–516 (2015).

20. M. K. Akhlaghi, A. H. Majedi, and J. S. Lundeen, "Nonlinearity in single photon detection: modeling and quantum tomography," Opt. Express **19**(22), 21305–21312 (2011).

21. F. Piacentini, M. P. Levi, A. Avella, M. López, S. Kück, S. V. Polyakov, I. P. Degiovanni, G. Brida, and M. Genovese, "Positive operator-valued measure reconstruction of a beam-splitter tree-based photon-number-resolving detector," Opt. Lett. **40**(7), 1548–1551 (2015).

22. M. Itzler, X. Jiang, M. Entwistle, K. Slomkowski, A. Tosi, F. Acebi, F. Zappa, and S. Cova, "Advances in InGaAsP-based avalanche diode single photon detectors," J. Mod. Opt. **58**(3-4), 174–200 (2011).

23. C. Scarcella, G. Boso, A. Ruggeri, and A. Tosi, "InGaAs/InP single-photon detector gated at 1.3 GHz with 1.5% afterpulsing," IEEE J. Sel. Top. Quantum Electron. **21**(3), 17 (2015).

24. C. Hughes, M. Genoni, T. Tufarelli, G. Matteo, and M. Kim, "Quantum non-Gaussianity witnesses in phase space," Phys. Rev. A **90**(1), 013810 (2014).

25. V. D'Auria, O. Morin, C. Fabre, and J. Laurat, "Effect of the heralding detector properties on the conditional generation of single-photon states," Eur. Phys. J. D **66**(10), 249 (2012).

26. J. Lundeen, A. Feito, H. Coldenstrodt-Ronge, K. Pregnell, C. Silberhorn, T. Ralph, J. Eisert, M. Plenio, and I. Walmsley, "Tomography of quantum detectors," Nat. Phys. **5**(1), 27–30 (2009).

27. T. Amri, J. Laurat, and C. Fabre, "Characterizing quantum properties of a measurement apparatus: insights from the retrodictive approach," Phys. Rev. Lett. **106**(2), 020502 (2011).

28. G. Ichikawa, S. Komamiya, Y. Kamiya, Y. Minami, M. Tani, P. Geltenbort, K. Yamamura, M. Nagano, T. Sanuki, S. Kawasaki, M. Hino, and M. Kitaguchi, "Observation of the spatial distribution of gravitationally bound quantum states of ultracold neutrons and its derivation using the Wigner function," Phys. Rev. Lett. **112**(7), 071101 (2014).

1. Introduction

Near-infrared single-photon detectors play a significance role in a wide range of applications, such as quantum key distribution [1–5], laser ranging [6–9] and biological fluorescence imaging [10]. In particular, InGaAs/InP avalanche photodiodes (APDs) operating in gated Geiger-mode are widely used in the near-infrared single-photon detection due to the compact structure and the non-cryogenic cooling. However, the short gating pulses would cause the so-called spike noise due to the charging and discharging on the capacitance of the APD, and the weak photon-induced avalanche signals are usually buried in the spike noise. So far, various techniques have been proposed to discriminate the avalanche signals from noise. For instance the self-differencing technique [11–13] and the sinusoidal gating technique [14,15] enabled to increase the gate repetition rate up to GHz. Thanks to these advances, single-photon detectors based on InGaAs/InP APDs have already demonstrated a desirable performance for single-photon-level sensing at high speed. Due to the ever-growing need for the high-speed infrared single-photon detection in different applications, especially in quantum optics such as quantum key distribution [1–5], quantum state engineering based on conditional measurement [16] and linear optical quantum computing [17], it is necessary to assess the complete features of quantum detectors [18]. The quantum measurement such as quantum state tomography has become an important tool for the realization of diverse applications which require non-

classical state as the resource [19], by which we can use the known input state to characterize the detector [20, 21].

In this paper, we experimentally demonstrate and characterize a high-speed single-photon detector working at a high repetition rate up to 60 MHz, and a peak detection efficiency of 34% has been achieved with a dark count rate of 9×10^{-3} per gate. The detector was operated based on the capacitance balancing technique where a variable capacitance was employed in the spike noise cancellation circuit to simulate the APD's spike noise generated during the charging-discharging process. Such technique finally provided a high noise suppression up to 11 dB. In contrast to other techniques, the circuits of the capacitance balancing detectors could operate at variable gating-frequency from 10 MHz to 60 MHz. For the quantum characterization of this kind of detector, positive operator valued measure (POVM) formalism were thus introduced here. Experimentally, we sent a set of various known coherent states generated by an attenuated pulsed laser to determine the POVM elements. Alternatively, the POVM elements of an on/off photon detector could also be given by the detection efficiency and dark noise. In our experiment, these POVM elements obtained by these two methods exhibit a good agreement. From the POVM elements, the corresponding Wigner function were thus given to witness the quantum feature of the detector. Moreover, we also observed quantum decoherence of the photon detector by increasing the bias voltage, thus demonstrating a transition from the full-quantum to semi-classical regime. The understanding and the control of this dynamic process may be of crucial importance in mastering the quantum information processing and quantum state engineering [16].

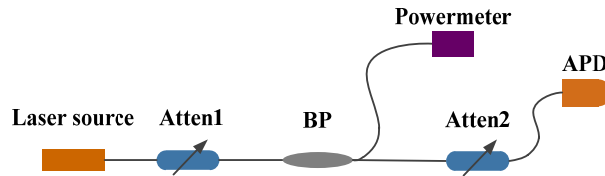## 2. Characterization of the single photon detector

Fig. 1. Experimental setup of the detector tomography. Atten1,2: attenuators; BP: beam splitter; Laser source: a continuous-wave laser or a pulsed laser at 1550 nm.

The detector based on InGaAs/InP APD we used here could be operated in the gated Geiger mode with a variable gating frequency from 10 MHz to 200 MHz without changing any external conditions. The detection window was set to 1 ns. Since the short gating pulses would cause spike noise by charging and discharging on the capacitance of the APD, we employed a variable capacitor to generate an imitated spike noise for cancellation. The APD and the complementary capacitor stayed in parallel in the circuit with a high reverse voltage applied on them. The response signals of the APD and the capacitor from each gate combined in the magic-T network [22, 23], which contained a transformer to do the subtraction. By this transformer, the two spikes cancelled each other due to a π phase difference and then the avalanche signals could be extracted. Such technique finally gave a high noise suppression up to 11 dB.

Firstly, we measured the saturated counting rate (SCR) of the detector as a function of the repetition rate of the gating pulse to find out the temporal response limit of the APD. The experimental setup is shown in Fig. 1. We used an attenuated continuous-wave laser as the laser source. The incident laser power was attenuated to about 1 μW, ensuring that more than 10^3 photons were contained in each detection gate. Tuning the gate repetition rate from 20 MHz to 90 MHz, we recorded the SCR at different gate repetition rates. As shown in Fig. 2, there is a linear rise of SCR with the increase of gate rate till 60 MHz. However, when the gate rate further increased, the SCR could not catch up with it. The increasing of the gate rate might shorten the avalanche build-up time which caused the loss of the SCR. Accordingly, we

could deduce that the dead time of the detector was about 16.7 ns which was the duration between two gates when the repetition rate was 60 MHz. The linearity in the detector response could not be guaranteed at the gate rate beyond 60 MHz. The tomography under this case could not be normally operated because of the unreachable maximum detective probability. To avoid the missing counting caused by the APD's temporal response limit, we set the gating pulse repetition rate at 60 MHz.
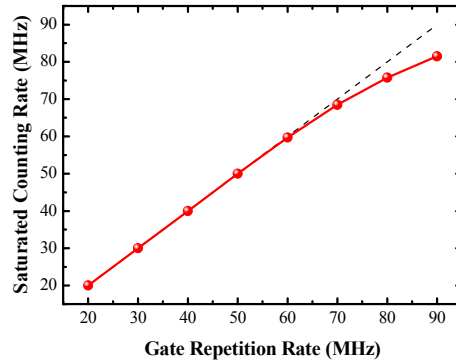

Fig. 2. Saturated counting rate as a function of the gate repetition rate. We illuminated the APD by an attenuated continuous-wave laser to ensure that more than 10^3 photons were contained in each detection window which duration was set to be 1 ns.

To characterize the detector, we replaced the continuous laser by a picosecond pulsed laser (PicoQuant PDL 800-B) in Fig. 1 to serve as the laser source with a wide modulation bandwidth, working at 1550 nm. We illuminated the detector with 0.1 photons/pulse by using the pulsed laser, and adjusted the bias voltage to 47.03 V to reach an about 600 kcounts/s, by which the efficiency of the detector was set to 10%. Then we turned off the pulsed laser to record that the dark count rate (DCR) was 7.1×10^{-6} per gate.

For the quantum tomography measurement, the experimental setup was the same as in the classical characterization in Fig. 1. We used the picosecond pulsed laser as the laser source. The repetition rate of the laser pulse was set at 60 MHz. Then the laser pulses went through an adjustable intensity attenuator Atten1. With the attenuators we could adjust the photon flux of the incident light, i.e. the average photon number per pulse μ. We varied μ from 0 to 200. In order to monitor the incident light power, we put a 50:50 beam splitter into the optical path, an alternative output of this BP connected to the power meter for real-time monitoring. Then the light pulses went through Atten2 with a large constant attenuation (50 dB) to the single-photon level to illuminate the APD. The APD had two outcomes, either outputting an electronic pulse (1 click) or not (0 click).

To obtain the full quantum characterization of this detector, we performed the quantum detector tomography (QDT). We could find out the general description of a measurement apparatus by the POVM formalism in quantum mechanics [20]. Single photon detectors working in Geiger mode can be seen as on/off detectors, which means that outcomes of detection are either registering an electronic pulse (1 click) or not (0 click). A perfect on/off detector can be described by two POVM elements as $\hat{\Pi}_{off} = |0\rangle\langle0|$ and $\hat{\Pi}_{on} = \hat{1} - |0\rangle\langle0|$. However, in practical solution, detectors are unable to detect the incoming photons with unit probability. In addition, the performance of a realistic detector is also degraded by the presence of dark noise, we note v as the average photon number of dark noise per detection gate, then the general POVM elements for an on/off detector are thus rewritten as [24]:

$$\hat{\Pi}_{off} = e^{-v} \sum_{k=0}^{\infty} (1-\eta)^k |k\rangle\langle k|, \quad \hat{\Pi}_{on} = \hat{1} - \hat{\Pi}_{off}, \tag{1}$$

where η stands for optical detection efficiency. Disregarding after pulsing or dark counts, the coefficient $(1-\eta)^k$ is given by the reconstructed operator $\hat{\Pi}_{off}$ for an impinging Fock state $|k\rangle$ and it can be regarded as the probability that k photons are not detected under an efficiency of η. We can also consider it the probability of not detecting a photon when the magnitude of the incoming photon is k. So we could alter the average photon number per pulse μ by the variable attenuators to perform the detector tomography [25].
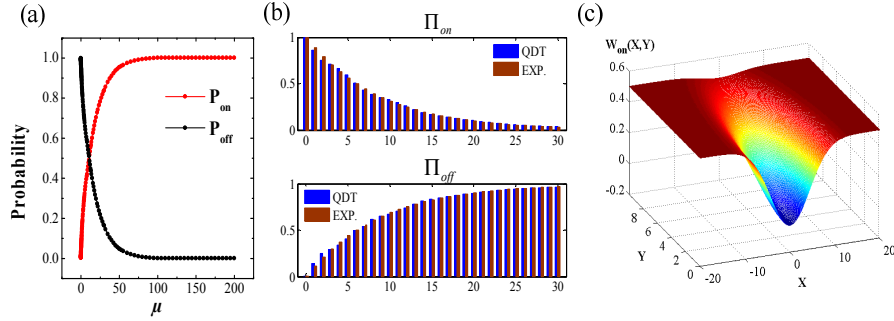

Fig. 3. (a) Measured probability distributions for different outcomes as a function of average photon per pulse. (b) Comparison of the POVM based on experimental measured η and v with the reconstructed POVM based on QDT. (c) Corresponding Wigner function for the representation of the POVM element Π_{on}.

Assuming the working state of the detector was unknown, we could have characterized it by measuring a set of known probe states $\{|k\rangle\}$ [26], i.e. Fock states. By tuning the average photon number per pulse μ continuously we recorded the probably of "having a click" P_{on}, i.e. one or more photon has been detected. Figure 3(a) provides us the probabilities of different situation as a function of the average photon number. We used the maximum likelihood algorithm [27] to reconstruct the POVM density matrices. Alternatively, we can also give the POVM elements based on the experimental measured η (10%) and v (7.1 × 10⁻⁶ per gate) according to Eq. (1). Figure 3(b) shows the reconstructed operators Π_{on} and Π_{off} by means of QDT and experiment, respectively, from which we could find a good agreement between experimental and theoretical data, indicating that the parameters of the detector measured by the conventional methods truly presented the features of the detector.

We can use the Wigner function of the reconstructed POVM elements to visualize the properties of the detector conveniently. Notice that the POVM operator given in Eq. (1), the general Wigner function can be rewritten in the form [28]

$$W_{on} = \frac{1}{2\pi\sigma_0^2} \left(\frac{1}{2} - \frac{e^{-v}}{2-\eta} e^{-(x^2+y^2)/2\sigma_\eta^2} \right), \tag{2}$$

where e^{-v} stands for the mean photon number of noise in each detection window. Figure 3(c) shows the corresponding Wigner function. The value of this function (−0.026) is negative at the origin of coordinate, which is a signature of full-quantum nature of the measurement, indicating that this detector is a fundamentally quantum detector under this operation situation.

3. Quantum decoherence of the detector

In the following, we turn to investigate the performance of the detector at different bias voltages. Figure 4(a) provides the evolutions of detection efficiency and DCR as a function of the bias voltage, and Fig. 4(b) shows the partial Wigner functions for four different situations, respectively. The variation of the detection efficiency and the DCR indicates that the bias voltage had a great effect on the detector's performance. As shown in Fig. 4(a), when the bias voltage was below 49.05 V, the detection efficiency increased with the bias voltage. Meanwhile, the DCR was kept at a very low level. Correspondingly, as shown in Table 1, with an applied bias voltage of 47.03 V, the value of Wigner function at the origin was −0.026. Although the detection efficiency was as low as 10%, this value stayed negative under such a low bias voltage, which mainly benefited from the low DCR. Figure 4(b) exhibits that when the bias voltage was 49.05 V, the negative value of W_{on} achieved its minimum −0.097 when the efficiency reached as high as 34%. Above this bias voltage, we could observe clearly that the detection efficiency degraded sharply and DCR rose quickly.
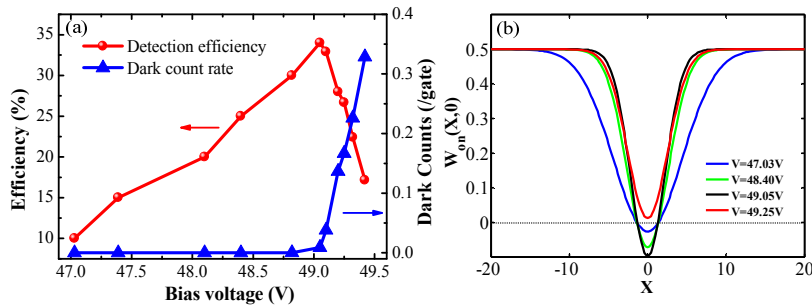

Fig. 4. (a) Single-photon detection efficiency and dark counts as a function of bias voltage applied on the APD. (b) Cross sections of the Wigner function of the detector under different bias voltages.

With the rising of the bias voltage, the negativity of W_{on} at the origin rose gradually until the detection efficiency began to drop, as shown in Table 1. We further augmented the bias voltage and found that this negativity didn't increase any more but began to decline rapidly, and finally disappeared. Here the detector was driven away from the full-quantum regime which could be called "quantum decoherence". We noticed that the disappearance occurred at 49.25 V with the function value of 0.012, meanwhile the DCR rose up to 0.17 per gate. Using Eq. (2), we could obtain the exact boundary between the two different regimes for the single-photon detector used here as $v = -\ln(1-\eta/2)$. In the experiment, the border of this negativity is between these two working point: $\eta = 28.0\%$, $v = 0.14$ and $\eta = 26.7\%$, $v = 0.17$, which are in agreement with the experimental result.

Table 1. Values of Wigner function at the origin of coordinate with different bias voltages.

Voltage (V)	Efficiency (%)	DCR (/gate)	DCR (counts/s)	Won(0,0)
47.03	10.0	7.1×10^{-6}	426	−0.026
48.40	25.0	6.4×10^{-5}	3840	−0.071
49.05	34.0	9×10^{-3}	5.4×10^{5}	−0.097
49.10	32.9	3.8×10^{-2}	2.28×10^{6}	−0.076
49.20	28.0	1.4×10^{-1}	8.4×10^{6}	−0.007
49.25	26.7	1.7×10^{-1}	1.02×10^{7}	0.012

In Table 1, with the efficiency of the detector increasing from 10% to 34%, the value of W_{on} decreased to its minimum though the DCR increased. We could find that the efficiency improvement was the dominant influence factor on $W_{on}(0,0)$. After that, the significant increasing of DCR played a more important role in the gradual disappearance of the W_{on} negative value. We could also find the great influence of DCR in two situations with bias voltage of 48.40 V and 49.20 V in Table 1, the corresponding detection efficiency were 25% and 26.7%, the DCR were 6.4×10^{-5}/gate and 1.7×10^{-1}/gate, respectively. The increasing of DCR led to the transition of the value of $W_{on}(0,0)$ from negative to positive when the detection efficiency varied slightly.

With the bias voltage of 49.05 V, the negative value of $W_{on}(0,0)$ attained its minimum, which is a strong signature of full-quantum features. Therefore, when the bias voltage was set at 49.05 V, the detector was at its optimal operation. We also observed a negative to positive transition of Wigner function which in a quantitative way indicated a degradation of detector's performance.

4. Conclusion

Based on the capacitance-balancing technique, the spike noise of the single-photon detector was much suppressed. The gate repetition rate of the single-photon detector would be tuned from 10 MHz to 60 MHz with a low noise kept at 10^{-6} per gate level when the detection efficiency varied from 0 to 20%. In order to characterizing the detector under different conditions, we implemented the quantum tomography at 60 MHz of repetition rate and for the detection window of 1 ns and determined its POVM. With the Wigner function, an explicit evolution of the detector's behavior from the full-quantum to semi-classical regime could be witnessed and the exact border between two different regimes could be obtained. Operating at 60 MHz and under a bias voltage of 49.05 V, the detector could reach an efficiency of 34% with the DCR of 0.009 per gate, during which W_{on} reached its minimum negative value, indicating the quantum properties of the detector. The excellent quantum properties of the detector lead to a bright application future in quantum state engineering.